Engineering Analysis with Boundary Elements 54 (2015) 13–18

Contents lists available at ScienceDirect

Engineering Analysis with Boundary Elements

journal homepage: www.elsevier.com/locate/enganabound

# The solution to an elliptic partial differential equation for facilitating exact volume integral transformation in the 3D BEM analysis

Y.C. Shiah [a], Meng-Rong Li [b,*]

[a] Department of Aeronautics and Astronautics, National Cheng Kung University, Tainan 701, Taiwan
[b] Department of Mathematical Sciences, National Chengchi University, Taipei, Taiwan

ARTICLE INFO

*Article history:*
Received 14 August 2014
Received in revised form
13 December 2014
Accepted 18 December 2014
Available online 4 February 2015

*Keywords:*
Partial differential equation
Exact volume integral transformation
Boundary element analysis
3D anisotropic elasticity
Body-force effect

ABSTRACT

In the direct boundary element method (BEM), the body-force or its equivalence will reveal itself as a volume integral that shall destroy the important notion of boundary discretisation. For resolving this issue, the most elegant approach would be to analytically transform the volume integral to boundary ones. In the process of such attempt for 3D anisotropic elastostatics, the key lies in analytically formulating the fundamental solution to a partial differential equation. In this paper, the partial differential equation is presented in an elliptic form, followed by formulating its analytical solution. In the BEM analysis, the formulated solution will be a key part to the success of performing exact volume-to-surface integral transformation.



## 1. Introduction

Among all numerical tools, the BEM has been recognized as an efficient technique due to its distinctive feature that only the boundary needs to be discretised. This approach has been extensively applied to various disciplines of engineering analysis. However, when the analysis involves body-force effect, there will appear a volume integral in the integral equation that will conventionally require domain discretisation. Undoubtedly, such mesh discretisation over the whole domain will destroy the distinctive feature of the BEM. Over the years, a significant amount of research has been devoted to resolving this issue, for example the domain fanning approach [1], the particular integral approach [2], the dual reciprocity method [3], the radial integration method [4], and the exact transformation method [5]. Among these approaches, the exact transformation method, abbreviated as ETM herein, is the most appealing since it is analytically exact. Although analytically elegant, such approach to deal with 2D anisotropic elastostatics involving the body-force effect was not so successful until Zang et al. [6] presented general transformed boundary integrals. Based on such treatment, Shiah and Tan [7] further presented the transformed boundary integrals for computing interior stresses in 2D anisotropic bodies, being subjected to body forces. Despite the elegance and computational efficiency of the ETM, such treatment has still remained unexplored for dealing with body-force in 3D generally anisotropic elasticity ever since it was proposed decades before. Perhaps, the work by Shiah and Tan [8] is the only one in the open literature that applies the ETM to treat the domain integral, albeit for the thermoelastic effect in 3D transversely isotropic bodies.

The main difficulty for applying the ETM to 3D anisotropic elastostatics involving the body-effect is derived from the mathematical complexity of its Green's function. The seminary work for Green's function of 3D general anisotropic elasticity can be traced early back to 1947 [9], where it was expressed as a contour integral around a unit circle on an oblique plane. Since then, lots of researches have been devoted to deriving more explicit expressions (see e.g. [10–15]). Unlike what the others did previously, Shiah et al. [16] and Tan et al. [17] implemented the fundamental solutions presented by Ting and Lee [18] for displacements and those by Lee [19] for their first-order derivatives to form the solution of tractions in the BEM analysis for 3D generally anisotropic elasticity. For further simplifying their explicit expressions and boosting the computational efficiency, Shiah et al. [20] presented Fourier-series formulations for the fundamental solutions in the BEM analysis. The most appealing advantage of applying Fourier-series approach principally lies in the simplicity of the formulations, thus greatly enhancing the efficiency in computations.

For the present work, the newly introduced fundamental solution to the partial differential equation, presented in an elliptical form, is derived to facilitate the ETM. At the end,

* Corresponding author. Tel.: +886 2 2939309x88055.
*E-mail address:* liwei@math.nccu.edu.tw (M.-R. Li).

http://dx.doi.org/10.1016/j.enganabound.2014.12.011
0955-7997/

satisfaction of the constrained condition for the new fundamental solution is demonstrated by numerical tests. As speaks itself, the fundamental solution formulated plays a crucial role for the ETM, laying down the cornerstone for treating the body-force effect in 3D anisotropic elasticity.

## 2. BEM for 3D anisotropic elasticity

Before presenting the fundamental derivations, a brief review of the direct formulation of the BEM for treating 3D anisotropic elasticity is outlined first. The boundary integral equation, often abbreviated as BIE, to relate the nodal displacements $u_j$ and tractions $t_j$ on the boundary $S$ is expressed in indicial notation as

$$C_{ij}\,u_i(P)+\int_S u_i(Q)T_{ij}(P,Q)dS=\int_S t_i(Q)\,U_{ij}(P,Q)dS+\int_\Omega X_i(q)\,U_{ij}(P,\,q)d\Omega, \tag{1}$$

where $C_{ij}(P)$ is the geometrical coefficient at the source point $P$ on boundary, $X_i$ denotes the components of the equivalent body-force, $U_{ij}(P,Q)\equiv\mathbf{U}$ represents the fundamental solutions of displacements, and $T_{ij}(P,Q)$ stands for the fundamental solutions of tractions. In Eq. (1), the last term is a volume integral for an arbitrary field point $q$ in the domain $\Omega$, and direct integration of the volume integral by any conventional schemes shall require domain discretisation. Thus, the obvious goal is to transform it into boundary integrals that will restore the BEM feature of boundary discretisation. For simplicity, it is denoted by $V_j$ as follows:

$$V_j=\int_\Omega X_i U_{ij}(P,q)d\Omega \tag{2}$$

Computations of $\mathbf{U}$ proposed by Ting and Lee [18] have been discussed in Shiah et al. [16] and thus, only a brief review is provided herein for completeness. As presented by Ting and Lee [18], the explicit form of Green's function can be expressed as

$$\mathbf{U}(\mathbf{x})=\frac{1}{4\pi r}\frac{1}{|\boldsymbol{\kappa}|}\sum_{n=0}^{4}q_n\hat{\mathbf{\Gamma}}^{(n)}, \tag{3}$$

where $r$ represents the radial distance between the source point $P$ and the field point $Q$; $q_n$, $\hat{\mathbf{\Gamma}}^{(n)}$, and $\boldsymbol{\kappa}$ are given by

$$q_n=\begin{cases}\frac{-1}{2\beta_1\beta_2\beta_3}\left[\mathrm{Re}\left\{\sum_{t=1}^{3}\frac{p_t^n}{(p_t-\overline{p}_{t+1})(p_t-\overline{p}_{t+2})}\right\}-\delta_{n2}\right] & for\ \ n=0,1,2,\\ \frac{1}{2\beta_1\beta_2\beta_3}\mathrm{Re}\left\{\sum_{t=1}^{3}\frac{p_t^{n-2}\overline{p}_{t+1}\overline{p}_{t+2}}{(p_t-\overline{p}_{t+1})(p_t-\overline{p}_{t+2})}\right\} & for\ \ n=3,4,\end{cases} \tag{4a}$$

$$\hat{\Gamma}_{ij}^{(n)}=\tilde{\Gamma}_{(i+1)(j+1)(i+2)(j+2)}^{(n)}-\tilde{\Gamma}_{(i+1)(j+2)(i+2)(j+1)}^{(n)}\quad(i,j=1,2,3), \tag{4b}$$

$$\kappa_{ik}=C_{ijks}\mathrm{m}_j\mathrm{m}_s,\quad \mathbf{m}=(-\ \sin\theta,\ \cos\theta,0). \tag{4c}$$

In Eq. (4c), the spherical angle $\theta$ is as defined in Fig. 1; the Stroh eigenvalues, $p_i$, in Eq. (4a) appear as three pairs of complex conjugates. These quantities are expressed as

$$p_\nu=\alpha_\nu+i\,\beta_\nu,\quad \beta_\nu>0\quad(\nu=1,\,2,\,3) \tag{5}$$

with an over-bar on it denoting the corresponding conjugate. Also, in Eq. (4c), $C_{ijks}$ are the stiffness coefficients of material. In terms of the spherical coordinates as shown in Fig. 1, Green's function can be re-expressed as

$$\mathbf{U}(r,\theta,\phi)=\frac{\mathbf{H}(\theta,\phi)}{4\pi r}, \tag{6}$$

where $\mathbf{H}(\theta,\phi)$, referred to as the Barnett–Lothe tensor, only depends on the spherical angles $(\theta,\phi)$ as defined in Fig. 1.

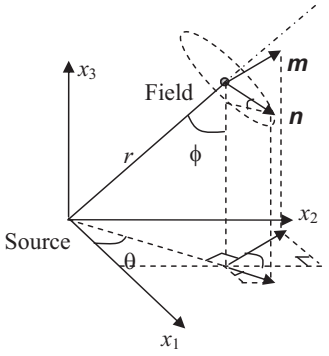


**Fig. 1.** Unit circle on the oblique plane at the field point.

Instead of computing the Bartnett–Lothe tensor directly, Shiah et al. [20] have very recently proposed to rewrite it as a double Fourier-series as follows:

$$H_{uv}(\theta,\phi)=\sum_{m=-\alpha}^{\alpha}\sum_{n=-\alpha}^{\alpha}\lambda_{uv}^{(m,n)}\,\mathrm{e}^{\mathrm{i}(m\theta+n\phi)}\quad(u,\ v=1,\ 2,\ 3), \tag{7}$$

where $\alpha$ is an integer large enough to ensure convergence of the series; $\lambda_{uv}^{(m,n)}$ are unknown coefficients determined, from the theory of Fourier series, by

$$\lambda_{uv}^{(m,n)}=\frac{1}{4\pi^2}\int_{-\pi}^{\pi}\int_{-\pi}^{\pi}H_{uv}(\theta,\phi)\mathrm{e}^{-\mathrm{i}(m\theta+n\phi)}d\theta\,d\phi. \tag{8}$$

The integral in Eq. (8) can be numerically evaluated, for example, by the Gaussian quadrature scheme to give

$$\lambda_{uv}^{(m,n)}=\frac{1}{4}\sum_{p=1}^{k}\sum_{q=1}^{k}w_p w_q f_{uv}^{(m,n)}\left(\pi\xi_p,\pi\xi_q\right), \tag{9}$$

where $k$ is the number of the Gauss abscissa $\xi_p$, and $w_p$ is the corresponding weight; $f_{uv}^{(m,n)}(\theta,\phi)$ represents the integrand in Eq. (8). Each computation of $\lambda_{uv}^{(m,n)}$ requires the evaluation of $H_{uv}(\theta,\phi)$ at points $(\pi\,\xi_p,\ \pi\,\xi_q)$ using Eqs. (3)–(5). For large values of $m$ and $n$, the rapid fluctuations of $f_{uv}^{(m,n)}(\theta,\phi)$ as shown in Shiah et al. [20] makes it usually necessary to use a relatively large number of Gauss points to accurately perform the numerical integrations. Generally, $k=64$ is sufficiently large to guarantee accurate integrations for obtaining convergent $\mathbf{H}(\theta,\phi)$ of a very generally anisotropic material. Since the computation of the Fourier coefficients by Eq. (9) is carried out only once irrespective of the number of field points in an engineering analysis, the CPU-time for this process is indeed very trivial in a complete BEM analysis of a problem.

For the first order derivatives of $\mathbf{U}$, denoted by $\mathbf{U}'$, the exact explicit algebraic expressions have been presented by Lee [19]. Instead, $\mathbf{U}'$ may be directly formulated by

$$\mathbf{U}'\equiv U_{uv,l}=\frac{\partial U_{uv}}{\partial r}\frac{\partial r}{\partial x_l}+\frac{\partial U_{uv}}{\partial\theta}\frac{\partial\theta}{\partial x_l}+\frac{\partial U_{uv}}{\partial\phi}\frac{\partial\phi}{\partial x_l}. \tag{10}$$

By direct differentiations using Eq. (13), the first order derivatives may be readily shown to have the following Fourier-series forms [20]:

$$U_{uv,l}=\frac{1}{4\pi r^2}\left\{\sum_{m=-\alpha}^{\alpha}\sum_{n=-\alpha}^{\alpha}\lambda_{uv}^{(m,n)}\,\mathrm{e}^{\mathrm{i}(m\theta+n\phi)}\begin{bmatrix}-\cos\theta(\sin\phi-\mathrm{i}n\cos\phi)\\ -\mathrm{i}m\sin\theta/\sin\phi\end{bmatrix}\right.$$

$$\text{for } l=1\ \sum_{m=-\alpha}^{\alpha}\sum_{n=-\alpha}^{\alpha}\lambda_{uv}^{(m,n)}\,\mathrm{e}^{\mathrm{i}(m\theta+n\phi)}\begin{bmatrix}-\sin\theta(\sin\phi-\mathrm{i}n\cos\phi)\\ +\mathrm{i}m\cos\theta/\sin\phi\end{bmatrix}$$

$$\text{for } l=2\ \sum_{m=-\alpha}^{\alpha}\sum_{n=-\alpha}^{\alpha}\lambda_{uv}^{(m,n)}\,\mathrm{e}^{\mathrm{i}(m\theta+n\phi)}[-(\cos\phi+\mathrm{i}n\sin\phi)]$$

$$\text{for } l=3. \tag{11}$$

As explained by Shiah et al. [20], the singularity issue at $\phi=0$ or $\pi$ in Eq. (11) may be resolved by simply using coordinate

transformation and thus, no further discussions are provided on this. As described in [20], the use of $\alpha=16$ will be sufficient to yield results with great accuracy. By the foregoing Fourier-series representations, the process of the exact transformation of the volume integral will be elaborated next.

## 3. Exact transformation of the volume integral

As has been well known, thermal effect can be treated as equivalent body-force in the BEM, resulting in an additional volume integral

$$V_j = -\int_{\Omega} \gamma_{ik}\Theta_{,k}(q)U_{ij}(P,q)d\Omega, \tag{12}$$

where $\gamma_{ik}$ are the thermal moduli; $\Theta$ stands for the temperature change in anisotropic media. By a very similar treatment as proposed by Shiah and Tan [7], Eq. (12) may be rewritten as

$$V_j = -\int_{\underline{\Omega}} \underline{\Gamma_{ik}}\Theta_{\underline{,k}}(q)U_{\underline{ij}}(P,q)d\underline{\Omega}, \tag{13}$$

where the symbol of underline is used to denote definitions in the new coordinates; $\underline{\Gamma_{ik}}$ are defined by

$$\underline{\Gamma_{ik}} = K_{11}\sqrt{\frac{\omega}{\Delta^3}}\begin{pmatrix}\gamma_{11} & \gamma_{12} & \gamma_{13}\\ \gamma_{21} & \gamma_{22} & \gamma_{23}\\ \gamma_{31} & \gamma_{32} & \gamma_{33}\end{pmatrix}\begin{pmatrix}\sqrt{\Delta}/K_{11} & -K_{12}/K_{11} & \alpha\\ 0 & 1 & \beta\\ 0 & 0 & \gamma\end{pmatrix}. \tag{14}$$

In Eq. (14), $K_{ij}$ denote the thermal conductivity coefficients of the anisotropic medium and the other coefficients are defined as follows:

$$\Delta = K_{11}K_{22} - {K_{12}}^2 > 0, \tag{15a}$$

$$\alpha = (K_{12}K_{13} - K_{23}K_{11})/\sqrt{\omega}, \tag{15b}$$

$$\beta = (K_{12}K_{23} - K_{13}K_{22})/\sqrt{\omega}, \tag{15c}$$

$$\gamma = \Delta/\sqrt{\omega}, \tag{15d}$$

$$\omega = K_{11}K_{13}\Delta - K_{11}K_{12}{K_{13}}^2 + K_{11}K_{12}K_{13}K_{23} - {K_{23}}^2{K_{11}}^2 > 0. \tag{15e}$$

As has been shown by Shiah and Tan [7] for 2D cases, the volume integral for problems without heat sources can be analytically transformed to surface ones, expressed as

$$V_j = \int_{\underline{S}} \underline{\Gamma_{ik}}\left[\left(\Theta W_{\underline{ijk},\underline{t}} - W_{\underline{ijk}}\Theta_{\underline{,t}}\right)n_{\underline{t}} - \Theta U_{\underline{ij}}n_{\underline{k}}\right]d\underline{S}, \tag{16}$$

where $W_{\underline{ijk}}$ is the new fundamental solution introduced according to

$$W_{\underline{ijk},\underline{tt}} = U_{\underline{ij},\underline{k}}. \tag{17}$$

Still, this transformation holds true for 3D cases if the above condition can be satisfied for the $U_{\underline{ij},\underline{k}}$, given by Eq. (11). Now, this brings forth the key part of the ETM process, viz Eq. (17) with the definition of Eq. (11), whose solution will be derived next.

## 4. Fundamental solution

As explicated previously, the crucial part to facilitate the transformation process lies in the solution to the partial differential equation in Eq. (17). Perhaps, this task seems very unlikely to achieve when Green's function is expressed as its original integral form [9]. However, with the recent development for expressing it as a simple Fourier-series representation [20], achieving this goal is no more that far away. The first step starts with expressing Eq. (11) as

$$U_{\underline{ij},\underline{k}} = \frac{1}{r^2}\kappa_{\underline{ijk}}(\theta,\phi), \tag{18}$$

where $\kappa_{\underline{ijk}}(\theta,\phi)$ is given accordingly by the equation itself. For the mathematical complexity of $U_{\underline{ij},\underline{k}}$, the challenge to seek the solution of $W_{\underline{ijk}}$ in Eq. (17) is obvious. For solving this partial differential equation, it is rewritten in the spherical coordinate system as

$$\frac{\partial^2 W_{\underline{ijk}}}{\partial r^2} + \frac{2}{r}\frac{\partial W_{\underline{ijk}}}{\partial r} + \frac{1}{r^2}\frac{\partial^2 W_{\underline{ijk}}}{\partial \phi^2} + \frac{\cot\phi}{r^2}\frac{\partial W_{\underline{ijk}}}{\partial \phi} + \frac{1}{r^2\sin^2\phi}\frac{\partial^2 W_{\underline{ijk}}}{\partial \theta^2} = \frac{\kappa_{\underline{ijk}}(\theta,\phi)}{r^2}, \tag{19}$$

where

$$\kappa_{\underline{ijk}}(\theta,\phi) = \frac{1}{4\pi}\Bigg\{ \sum_{m=-\alpha}^{\alpha}\sum_{n=-\alpha}^{\alpha}\lambda_{\underline{ij}}^{(m,n)}e^{i(m\theta+n\phi)}\begin{bmatrix} -\cos\theta(\sin\phi - in\cos\phi)\\ -im\sin\theta/\sin\phi\end{bmatrix}$$

$$for\ k=1,\ \sum_{m=-\alpha}^{\alpha}\sum_{n=-\alpha}^{\alpha}\lambda_{\underline{ij}}^{(m,n)}e^{i(m\theta+n\phi)}\begin{bmatrix} -\sin\theta(\sin\phi - in\cos\phi)\\ +im\cos\theta/\sin\phi\end{bmatrix}$$

$$for\ k=2,\ \sum_{m=-\alpha}^{\alpha}\sum_{n=-\alpha}^{\alpha}\lambda_{\underline{ij}}^{(m,n)}e^{i(m\theta+n\phi)}\left[-(\cos\phi + in\sin\phi)\right]$$

$$for\ k=3. \tag{20}$$

From Eq. (19), the $W_{ijk}$ can be written simply as $W_{ijk}(\theta,\phi)$, implying its independence of the radial distance $r$. Under the general condition when $\phi\neq 0$ or $\pi$, the factor $\sin^2\phi$ can be multiplied to the both sides of Eq. (19) to give

$$\sin^2\phi\frac{\partial^2 W_{\underline{ijk}}(\theta,\phi)}{\partial\phi^2} + \frac{\sin 2\phi}{2}\frac{\partial W_{\underline{ijk}}(\theta,\phi)}{\partial\phi} + \frac{\partial^2 W_{\underline{ijk}}(\theta,\phi)}{\partial\theta^2} = \kappa_{\underline{ijk}}(\theta,\phi)\sin^2\phi. \tag{21}$$

By making the following change of variables:

$$\eta = -\ln(|\csc\phi + \cot\phi|) \tag{22}$$

and assuming

$$\Lambda_1^{(m,n)}(\theta,\eta) = \frac{2e^{\eta}}{(1+e^{2\eta})^2}\left(2e^{\eta} - in\langle 1-e^{2\eta}\rangle\right)\cos\theta + im\sin\theta, \tag{23a}$$

$$\Lambda_2^{(m,n)}(\theta,\eta) = \frac{2e^{\eta}}{(1+e^{2\eta})^2}\left(2e^{\eta} - in\langle 1-e^{2\eta}\rangle\right)\sin\theta - im\cos\theta, \tag{23b}$$

$$\Lambda_3^{(n)}(\eta) = \frac{2}{1+e^{2\eta}}\left(1-e^{2\eta} + in\langle 2e^{\eta}\rangle\right), \tag{23c}$$

$$\Lambda_4^{(n)}(\eta) = \left(\frac{1-e^{2\eta}}{1+e^{2\eta}} + i\frac{2e^{\eta}}{1+e^{2\eta}}\right)^n, \tag{23d}$$

one may re-express Eq. (21) as

$$\frac{\partial^2 W_{\underline{ijk}}(\theta,\eta)}{\partial\theta^2} + \frac{\partial^2 W_{\underline{ijk}}(\theta,\eta)}{\partial\eta^2} = \kappa_{\underline{ijk}}(\theta,\phi), \tag{24}$$

where $\kappa_{\underline{ijk}}(\theta,\eta)$ is defined by

$$\kappa_{\underline{ijk}}(\theta,\eta) = \frac{-1}{4\pi}\begin{cases} \sum_{m=-\alpha}^{\alpha}\sum_{n=-\alpha}^{\alpha}\lambda_{\underline{ij}}^{(m,n)}\frac{2e^{\eta+im\theta}}{1+e^{2\eta}}\Lambda_4^{(n)}(\eta)\Lambda_1^{(m,n)}(\theta,\eta) & \text{for } k=1,\\ \sum_{m=-\alpha}^{\alpha}\sum_{n=-\alpha}^{\alpha}\lambda_{\underline{ij}}^{(m,n)}\frac{2e^{\eta+im\theta}}{1+e^{2\eta}}\Lambda_4^{(n)}(\eta)\Lambda_2^{(m,n)}(\theta,\eta) & \text{for } k=2,\\ \sum_{m=-\alpha}^{\alpha}\sum_{n=-\alpha}^{\alpha}\lambda_{\underline{ij}}^{(m,n)}\frac{2e^{2\eta+im\theta}}{(1+e^{2\eta})^2}\Lambda_4^{(n)}(\eta)\Lambda_3^{(m,n)}(\eta) & \text{for } k=3.\end{cases} \tag{25}$$

Taking advantage of the characteristic solution of a linear elliptic equation, one may give

$$W_{\underline{ij}1}(\theta,\eta)=\frac{1}{2\pi}\iint_{(s-\theta)^2+(r-\eta)^2\le\pi^2}\kappa_{\underline{ij}1}(r,s)\ln\sqrt{(s-\theta)^2+(r-\eta)^2}\,dr\,ds$$
$$=\frac{-1}{8\pi^2}\sum_{m=-\alpha}^{\alpha}\sum_{n=-\alpha}^{\alpha}\lambda_{\underline{ij}}^{(m,n)}\iint_{B_\pi(0,0)}e^{im(\theta+s)}\Lambda_4^{(n)}(\eta+r)I_1(\theta,\eta,r,s)$$
$$\ln\sqrt{s^2+r^2}\,dr\,ds, \tag{26}$$

where

$$I_1(\theta,\eta,r,s)=\frac{4e^{2(\eta+r)}}{\left(1+e^{2(\eta+r)}\right)^3}\left(2e^{(\eta+r)}-in\langle 1-e^{2(\eta+r)}\rangle\right)\cos(\theta+s)$$
$$+im\frac{2e^{(\eta+r)}}{1+e^{2(\eta+r)}}\sin(\theta+s) \tag{27a}$$

$$B_\pi(\theta,\eta)=\left\{(r,s):(s-\theta)^2+(r-\eta)^2\le\pi^2\right\}. \tag{27b}$$

As a result, one may obtain

$$W_{\underline{ij}1}(\theta,\phi)=\frac{-1}{8\pi^2}\sum_{m=-\alpha}^{\alpha}\sum_{n=-\alpha}^{\alpha}\lambda_{\underline{ij}}^{(m,n)}\iint_{B_\pi(0,0)}e^{im(\theta+s)}\Gamma_n(\phi,r)J_{\underline{1}}(\theta,\phi,r,s)$$
$$\ln\sqrt{s^2+r^2}\,dr\,ds, \tag{28}$$

where

$$\Gamma_n(\phi,r)=\left[\frac{1-(\sin\phi/(1+\cos\phi))^2e^{2r}}{1+(\sin\phi/(1+\cos\phi))^2e^{2r}}+i\frac{2|\sin\phi/(1+\cos\phi)|e^r}{1+(\sin\phi/(1+\cos\phi))^2e^{2r}}\right]^n, \tag{29a}$$

$$J_{\underline{1}}(\theta,\phi,r,s)=\frac{4(\sin\phi/(1+\cos\phi))^2e^{2r}}{[1+(\sin\phi/(1+\cos\phi))^2e^{2r}]^3}\left[2\left|\frac{\sin\phi}{1+\cos\phi}\right|e^r\right.$$
$$\left.-in\left\langle 1-\left(\frac{\sin\phi}{1+\cos\phi}\right)^2e^{2r}\right\rangle\right]\cos(\theta+s)$$
$$+im\frac{2|\sin\phi/(1+\cos\phi)|e^r}{1+(\sin\phi/(1+\cos\phi))^2e^{2r}}\sin(\theta+s). \tag{29b}$$

By the similar treatment, $\hat{W}_{\underline{ij}2}(\theta,\eta)$ is given by

$$W_{\underline{ij}2}(\theta,\eta)=\frac{1}{2\pi}\iint_{(s-\theta)^2+(r-\eta)^2\le\pi^2}\kappa_{\underline{ij}2}(r,s)\ln\sqrt{(s-\theta)^2+(r-\eta)^2}\,dr\,ds$$
$$=\frac{-1}{8\pi^2}\sum_{m=-\alpha}^{\alpha}\sum_{n=-\alpha}^{\alpha}\lambda_{\underline{ij}}^{(m,n)}\iint_{B_\pi(0,0)}e^{im(\theta+s)}\Lambda_4^{(n)}(\eta+r)I_2(\eta+r,\theta+s)$$
$$\ln\sqrt{s^2+r^2}\,dr\,ds, \tag{30}$$

where

$$I_2(\eta,\theta)=\frac{4e^{2r}}{\left(1+e^{2r}\right)^3}\left(2e^r-in\langle 1-e^{2r}\rangle\right)\sin s-im\frac{2e^r}{1+e^{2r}}\cos s. \tag{31}$$

Thus, with the formulation given in Eq. (30), one has

$$W_{\underline{ij}2}(\theta,\phi)=\frac{-1}{8\pi^2}\sum_{m=-\alpha}^{\alpha}\sum_{n=-\alpha}^{\alpha}\lambda_{\underline{ij}}^{(m,n)}\iint_{B_\pi(0,0)}e^{im(\theta+s)}\Gamma_n(\phi,r)J_{\underline{2}}(\theta,\phi,r,s)$$
$$\ln\sqrt{s^2+r^2}\,dr\,ds, \tag{32}$$

where

$$J_{\underline{2}}(\theta,\phi,r,s)=\frac{4(\sin\phi/(1+\cos\phi))^2e^{2r}}{[1+(\sin\phi/(1+\cos\phi))^2e^{2r}]^3}\left[2\left|\frac{\sin\phi}{1+\cos\phi}\right|e^r\right.$$
$$\left.-in\left\langle 1-\left(\frac{\sin\phi}{1+\cos\phi}\right)^2e^{2r}\right\rangle\right]\sin(\theta+s)$$
$$-im\frac{2|\sin\phi/(1+\cos\phi)|e^r}{1+(\sin\phi/(1+\cos\phi))^2e^{2r}}\cos(\theta+s). \tag{33}$$

Also, $W_{\underline{ij}3}(\theta,\eta)$ is given in a similar manner by

$$W_{\underline{ij}3}(\theta,\eta)=\frac{1}{2\pi}\iint_{(s-\theta)^2+(r-\eta)^2\le\pi^2}\kappa_{\underline{ij}3}(r,s)\ln\sqrt{(s-\theta)^2+(r-\eta)^2}\,dr\,ds$$
$$=\frac{-1}{4\pi^2}\sum_{m=-\alpha}^{\alpha}\sum_{n=-\alpha}^{\alpha}\lambda_{\underline{ij}}^{(m,n)}\iint_{B_\pi(0,0)}\frac{e^{2(\eta+r)+im(\theta+s)}}{(1+e^{2r})^2}\Lambda_3^{(n)}(\eta+r)\Lambda_4^{(n)}(\eta+r)$$
$$\ln\sqrt{s^2+r^2}\,dr\,ds. \tag{34}$$

In the sequel, the formulation in Eq. (34) gives

$$W_{\underline{ij}3}(\theta,\phi)=\frac{-1}{2\pi^2}\sum_{m=-\alpha}^{\alpha}\sum_{n=-\alpha}^{\alpha}\lambda_{\underline{ij}}^{(m,n)}\iint_{B_\pi(0,0)}e^{im(\theta+s)}\Gamma_n(\phi,r)J_{\underline{3}}(\phi,r)$$
$$\ln\sqrt{s^2+r^2}\,dr\,ds, \tag{35}$$

where

$$J_{\underline{3}}(\phi,r)=\frac{(\sin\phi/(1+\cos\phi))^2e^{2r}}{[1+(\sin\phi/(1+\cos\phi))^2e^{2r}]^3}\left[1-\left(\frac{\sin\phi}{1+\cos\phi}\right)^2e^{2r}\right.$$
$$\left.+in\left(\frac{\sin\phi}{1+\cos\phi}\right)^2e^{2r}\right]. \tag{36}$$

For brevity, the formulations derived above can be summarised as follows:

$$W_{\underline{ijk}}(\theta,\phi)=C_{\underline{k}}\sum_{m=-\alpha}^{\alpha}\sum_{n=-\alpha}^{\alpha}\lambda_{\underline{ij}}^{(m,n)}\iint_{B_\pi(0,0)}e^{im(\theta+s)}\Gamma_n(\phi,r)\hat{J}_{\underline{k}}(\theta/\phi,r/s)$$
$$\ln\sqrt{s^2+r^2}\,dr\,ds, \tag{37}$$

where $\Gamma_n(\phi,r)$ is given by Eq. (29a); $C_{\underline{k}}$, $\hat{J}_{\underline{k}}(\phi,r)$ are defined by

$$C_{\underline{k}}=\begin{cases}-1/8\pi^2 & \text{for } k=1,\ 2\\ -1/2\pi^2 & \text{for } k=3\end{cases}, \tag{38a}$$

$$\hat{J}_{\underline{k}}(\theta/\phi,r/s)=\begin{cases}J_{\underline{1}}(\theta,\phi,r,s) & \text{definedin Eq. (29b)},\\ J_{\underline{2}}(\theta,\phi,r,s) & \text{definedin Eq. (33)},\\ J_{\underline{3}}(\phi,r) & \text{definedin Eq. (36)}.\end{cases} \tag{38b}$$

Up to this point, the newly constructed fundamental solution has been completed provided with very explicit expressions; however, there is another issue regarding its numerical computations needed to be addressed. For numerical implementation in the BEM, evaluations of the fundamental solutions for millions of field points may be required and thus, direct computations using Eq. (37) may incur heavy computation burdens due to the integration. In principal, the periodic nature of the spherical angles still holds true for $W_{\underline{ijk}}(\theta,\phi)$, implying the existence of its Fourier-series form. For this, one may express it as the following Fourier-series:

$$W_{\underline{ijk}}(\theta,\phi)=\sum_{n=-\beta}^{\beta}\sum_{m=-\beta}^{\beta}\varpi_{\underline{ijk}}^{(m,n)}e^{i(m\theta+n\phi)}, \tag{39}$$

where

$$\varpi_{\underline{ijk}}^{(m,n)}=\frac{1}{4\pi^2}\int_{-\pi}^{\pi}\int_{-\pi}^{\pi}W_{\underline{ijk}}(\theta,\phi)e^{-i(m\theta+n\phi)}\,d\theta\,d\phi. \tag{40}$$

The above integration can be performed using any numerical scheme, for example the $\beta$-point Gauss quadrature rule as follows:

$$\varpi_{\underline{ijk}}^{(m,n)}=\frac{1}{4}\sum_{q=1}^{\beta}\sum_{p=1}^{\beta}w_pw_qf_{\underline{ijk}}^{(m,n)}(\pi\xi_p,\pi\xi_q), \tag{41}$$

where $f_{\underline{ijk}}^{(m,n)}$ represents the integrand in Eq. (40), namely

$$f_{\underline{ijk}}^{(m,n)}(\theta,\phi)=W_{\underline{ijk}}(\theta,\phi)e^{-i(m\theta+n\phi)}. \tag{42}$$

It is worth noting that this process of taking Fourier-series is performed only once, irrespective of the number of field points

**Table 1**
Comparison between $\nabla^2 W_{\underline{122}}(\theta,\phi)$ and $U_{\underline{12,2}}(\theta,\phi)$ for quartz and alumina.

| $(\theta, \phi)$ | Quartz | | $Al_2O_3$ | |
|---|---|---|---|---|
| | LHS ($\nabla^2 W_{122}$) | RHS($U_{12,2}$) | LHS($\nabla^2 W_{122}$) | RHS($U_{12,2}$) |
| (1.249046, 0.546376) | 1.446653E−04 (0.015%) | 1.446434E−04 | 4.955505E−05 (0.001%) | 4.955552E−05 |
| (1.892547, 0.546376) | 5.071006E−05 (0.005%) | 5.070744E−05 | −3.681205E−05 (0.001%) | −3.681182E−05 |
| (4.390639, 0.546376) | −1.827800E−04 (0.009%) | −1.827643E−04 | −5.365682E−05 (0.001%) | −5.365728E−05 |
| (5.034139, 0.546376) | −9.705379E−05 (0.001%) | −9.705292E−05 | 2.318588E−05 (0.002%) | 2.318625E−05 |
| (1.249046, −0.546376) | 1.827800E−04 (0.009%) | 1.827643E−04 | 5.365635E−05 (0.001%) | 5.365682E−05 |
| (1.892547, −0.546376) | 9.705292E−05 (0.000%) | 9.705292E−05 | −2.318550E−05 (0.004%) | −2.318643E−05 |
| (4.390639, −0.546376) | −1.446644E−04 (0.015%) | −1.446425E−04 | −4.955459E−05 (0.001%) | −4.955505E−05 |
| (5.034139, −0.546376) | −5.070936E−05 (0.005%) | −5.070682E−05 | 3.681214E−05 (0.001%) | 3.681242E−05 |
| (0.000000, 0.000000) | −3.368772E−03 (0.007%) | −3.369008E−03 | −4.159871E−03 (0.000%) | −4.159881E−03 |
| (0.000000, 3.141593) | 3.368772E−03 (0.007%) | 3.369017E−03 | 4.159876E−03 (0.000%) | 4.159881E−03 |

involved in the BEM analysis. In other words, having determined its coefficients via Eq. (41), one may directly compute $W_{\underline{ijk}}(\theta,\phi)$ for arbitrary field points by Eq. (39).

## 5. Numerical tests

For the test, the quartz with the following stiffness coefficients [21] defined in its principal directions, denoted by $\mathbf{C}^*$, is selected as the material:

$$\mathbf{C}^* = \begin{bmatrix} 87.6 & 6.07 & 13.3 & 17.3 & 0 & 0 \\ 6.07 & 87.6 & 13.3 & -17.3 & 0 & 0 \\ 13.3 & 13.3 & 106.8 & 0 & 0 & 0 \\ 17.3 & -17.3 & 0 & 57.2 & 0 & 0 \\ 0 & 0 & 0 & 0 & 57.2 & 17.3 \\ 0 & 0 & 0 & 0 & 17.3 & 40.765 \end{bmatrix} \text{GPa.} \quad (43)$$

As a result of successively rotating the principal axes by 30°, 45°, 60° around the $x_1$-, $x_2$-, $x_3$-axis clockwise, the corresponding stiffness coefficients in the global coordinate system turn out to have a fully populated matrix form

$$\mathbf{C} = \begin{bmatrix} 111.8 & 14.8 & -5.2 & -0.3 & 11.0 & -14.0 \\ 14.8 & 101.8 & -7.6 & 0.4 & -0.6 & 18.9 \\ -5.2 & -7.6 & 129.7 & 4.4 & 1.6 & 0.6 \\ -0.3 & 0.4 & 4.4 & 31.3 & 2.5 & 3.6 \\ 11.0 & -0.6 & 1.6 & 2.5 & 37.9 & 1.3 \\ -14.0 & 18.9 & 0.6 & 3.6 & 1.3 & 55.2 \end{bmatrix} \text{GPa.} \quad (44)$$

For verifying the validity of computations for different materials, the alumina ($Al_2O_3$) is selected as the second material for the check. In the principal directions, it has the stiffness coefficients:

$$\mathbf{C}^* = \begin{bmatrix} 465 & 124 & 117 & 0 & 0 & 0 \\ 124 & 465 & 117 & 0 & 0 & 0 \\ 117 & 117 & 563 & 0 & 0 & 0 \\ 0 & 0 & 0 & 233 & 0 & 0 \\ 0 & 0 & 0 & 0 & 233 & 0 \\ 0 & 0 & 0 & 0 & 0 & 170.5 \end{bmatrix} \text{GPa.} \quad (45)$$

The principal axes are rotated by 20°, 80°, 150° counterclockwise to yield the following generally anisotropic coefficients:

$$\mathbf{C} = \begin{bmatrix} 564.8 & 113.6 & 113.7 & -3.7 & -2.0 & -2.0 \\ 113.6 & 471.4 & 123.5 & 3.1 & -1.7 & 18.5 \\ 113.7 & 123.5 & 471.2 & 3.1 & 18.4 & -1.7 \\ -3.7 & 3.1 & 3.1 & 173.8 & 9.5 & 9.3 \\ -2.0 & -1.7 & 18.4 & 9.5 & 227.8 & -1.8 \\ -2.0 & 18.5 & -1.7 & 9.3 & -1.8 & 227.8 \end{bmatrix} \text{GPa.} \quad (46)$$

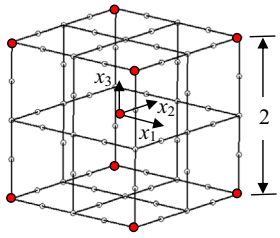


**Fig. 2.** A cubic domain defined in the global Cartesian coordinate.

Going through the processes using $\alpha=22$, the coefficients of $W_{ijk}(\theta,\phi)$ were computed. Now, the experiment is to check whether Eq. (17) may be satisfied by the computed coefficients for a few sample field points. This test was carried out for all 18 independent sets of $W_{ijk}(\theta,\phi)$ with different $i$, $j$, $k$ values. The left-hand-side of Eq. (17) was computed using the central difference scheme based on Eq. (37), while the right-hand-side was directly by Eq. (11); all computations are assumed to be performed in the new (underlined) coordinate system. Table 1 lists the comparison of the $W_{\underline{122}}(\theta,\phi)$ computed for a few sample field points using the RHS and LHS of Eq. (17). Since all the other components of $W_{ijk}(\theta,\phi)$ have similar percentages of difference, only the results for $W_{\underline{122}}(\theta,\phi)$ are shown here. As can be seen from the comparison, the percentages of difference between the both results are insignificant indeed.

For further verifying the validity of the volume-to-surface integral transformation, the next example considers a 2 (units) × 2 (units) × 2 (units) cube as schematically shown in Fig. 2. The material is arbitrarily assumed to have the following properties:

$$\mathbf{C} = \begin{bmatrix} 468.76 & 118.27 & 120.43 & -4.41 & 8.99 & 11.46 \\ 118.27 & 557.54 & 85.60 & 16.23 & -7.07 & 3.36 \\ 120.43 & 85.60 & 534.09 & 31.66 & 5.15 & -5.81 \\ -4.41 & 16.23 & 31.66 & 200.48 & 1.06 & -1.67 \\ 8.99 & -7.07 & 5.15 & 1.06 & 194.11 & 28.81 \\ 11.46 & 3.36 & -5.81 & -1.67 & 28.81 & 208.21 \end{bmatrix} \text{(Units),} \quad (47a)$$

$$\boldsymbol{\gamma} = \begin{bmatrix} 18.08 & 1.16 & 3.02 \\ 1.16 & 16.50 & 2.81 \\ 3.02 & 2.81 & 17.67 \end{bmatrix} \text{(Units),}$$

$$\mathbf{K} = \begin{bmatrix} 25.23 & 6.67 & 6.76 \\ 6.67 & 18.15 & -1.08 \\ 6.76 & -1.08 & 25.69 \end{bmatrix} \text{(Units).} \quad (47b)$$

**Table 2**
Comparison of the computed volume integral and the surface integrals.

| $(x_1, x_2, x_3)$ | $V_j$ by Eq. (12) | | | $V_j$ by Eq. (16) | | |
|---|---|---|---|---|---|---|
| | $j=1$ | $j=2$ | $j=3$ | $j=1$ | $j=2$ | $j=3$ |
| (−1.0, −1.0, −1.0) | 0.302432 | −0.260765 | 0.156997 | 0.302945 (0.17%) | −0.260314 (0.17%) | 0.157567 (0.36%) |
| (1.0,−1.0,−1.0) | 0.325770 | −0.320398 | 0.108081 | 0.325312 (0.14%) | −0.319271 (0.35%) | 0.10910 (0.94%) |
| (1.0,1.0,−1.0) | 0.230505 | −0.294819 | 0.134156 | 0.231071 (0.19%) | −0.295269 (0.15%) | 0.134491 (0.25%) |
| (−1.0,1.0,−1.0) | 0.299454 | −0.324789 | 0.165856 | 0.299640 (0.06%) | −0.324916 (0.04%) | 0.166046 (0.11%) |
| (−1.0,−1.0,1.0) | 0.263114 | −0.282511 | 0.136180 | 0.263928 (0.31%) | −0.281695 (0.29%) | 0.135568 (0.45%) |
| (1.0,−1.0,1.0) | 0.356946 | −0.361791 | 0.214370 | 0.355176 (0.50%) | −0.360592 (0.33%) | 0.212575 (0.84%) |
| (1.0,1.0,1.0) | 0.288918 | −0.298646 | 0.141088 | 0.288382 (0.19%) | −0.299141 (0.17%) | 0.140478 (0.43%) |
| (−1.0,1.0,1.0) | 0.315842 | −0.328789 | 0.075257 | 0.315937 (0.27%) | −0.329031 (0.21%) | 0.0750446 (0.09%) |

Temperature field is assumed to be distributed as follows:

$$\Theta(x_1, x_2, x_3) = (x_1+3)(x_2-2)(x_3+5). \tag{48}$$

Thus, the original volume integral defined in Eq. (12) was directly integrated using the 100-point Gauss quadrature scheme to acquire numerical accuracy for comparison. Also, the transformed boundary integrals in Eq. (16) were also computed using the 8-point Gauss quadrature scheme and the boundary discretisation (24 elements) as shown in Fig. 2. Table 2 lists the results computed using Eqs. (12) and (16). As can be seen from the comparison in Table 2, the discrepancies between the both are indeed very minor, which are mostly due to errors from numerical integrations.

## 6. Conclusive remarks

In the BEM analysis, the exact transformation of the additional volume integral arising from the body-force effect cannot be achieved unless the new fundamental solution, according to Green's 2nd-theorem, can be determined. In this paper, the new fundamental solution for 3D anisotropic elasticity is analytically derived by solving the partial differential equation obtained from Green's 2nd-theorem in the spherical coordinate system. The fundamental solution is formulated in a form of double integral. For facilitating its computations in the BEM implementation, the fundamental is further expressed as a Fourier-series, whose coefficients can be calculated only once, regardless of the number of field points involved for the computation. The formulations presented here can be regarded as a cornerstone for completing the process of the ETM for 3D anisotropic elasticity, and this is still under development as the future work.

## Acknowledgements

The authors gratefully acknowledge the financial support from the National Science Council of Taiwan (No. 102-2221-E-006–290-MY3).

## References

[1] Camp CV, Gipson GS. Boundary element analysis of nonhomogeneous biharmonic phenomena. Berlin: Springer-Verlag; 1992.
[2] Deb A, Banerjee PK. BEM for general anisotropic 2D elasticity using particular integrals. Commun Appl Num Methods 1990;6:111–9.
[3] Nardini D, Brebbia CA. A new approach to free vibration analysis using boundary elements. In: Boundary element methods in engineering. Southampton: Computational Mechanics Publications; 1982.
[4] Gao Xiao-Wei. The radial integration method for evaluation of domain integrals with boundary-only discretization. Eng Anal Bound Elem 2002;26:905–16.
[5] Rizzo FJ, Shippy DJ. An advanced boundary integral equation method for three-dimensional thermoelasticity. Int J Numer Methods Eng 1977;11:1753–1768.
[6] Zang JJ, Tan CL, Afagh FF. A general exact transformation of body-force volume integral in BEM for 2D anisotropic elasticity. Comput Mech 1996;19:1–10.
[7] Shiah YC, Tan CL. Calculation of interior point stresses in two-dimensional boundary element analysis of anisotropic bodies with body forces. J Strain Anal Eng Des 1998;34:117–28.
[8] Shiah YC, Tan CL. Boundary element method for thermoelastic analysis of three-dimensional transversely isotropic solids. Int J Solids Struct 2012;49:2924–2933.
[9] Lifshitz IM, Rosenzweig LN. Construction of the Green tensor for the fundamental equation of elasticity theory in the case of unbounded elastically anisotropic medium. Zh Eksp Teor Fiz 1947;17:783–91.
[10] Wilson RB, Cruse TA. Efficient implementation of anisotropic three dimensional boundary integral equation stress analysis. Int J Numer Methods Eng 1978;12:1383–97.
[11] Sales MA, Gray LJ. Evaluation of the anisotropic Green's function and its derivatives. Comp Struct 1998;69:247–54.
[12] Pan E, Yuan FG. Boundary element analysis of three dimensional cracks in anisotropic solids. Int J Numer Methods Eng 2000;48:211–37.
[13] Tonon F, Pan E, Amadei B. Green's functions and boundary element method formulation for 3D anisotropic media. Comp Struct 2001;79:469–82.
[14] Phan PV, Gray LJ, Kaplan T. On the residue calculus evaluation of the 3D anisotropic elastic Green's function. Comm Numer Methods Eng 2004;20:335–341.
[15] Wang CY, Denda M. 3D BEM for general anisotropic elasticity. Int J Solids Struct 2007;44:7073–91.
[16] Shiah YC, Tan CL, Lee VG. Evaluation of explicit-form fundamental solutions for displacements and stresses in 3D anisotropic elastic solids. Comput Model Eng Sci 2008;34:205–26.
[17] Tan CL, Shiah YC, Lin CW. Stress analysis of 3D generally anisotropic elastic solids using the boundary element method. Comput Model Eng Sci 2009;41:195–214.
[18] Ting TCT, Lee VG. The three-dimensional elastostic Green's function for general anisotropic linear elastic solid. Q J Mech Appl Math 1997;50:407–426.
[19] Lee VG. Derivatives of the three-dimensional Green's function for anisotropic materials. Int J Solids Struct 2009;46:*1471*–9.
[20] Shiah YC, Tan CL, Wang CY. Efficient computation of the Green's function and its derivatives for three-dimensional anisotropic elasticity in BEM analysis. Eng Anal Bound Elem 2012;36:1746–55.
[21] Nye JF. Physical Properties of Crystals, Their Representation by Tensors and Matrices. Oxford: Clarendon; 1960.